
All that structure matches does not glitter

**Maya M. Martirosyan^{1,2}, Thomas Egg^{1,2}, Philipp Höllmer^{1,2},
 George Karypis³, Mark Transtrum⁴, Adrian Roitberg^{5,6}, Mingjie Liu^{5,6},
 Richard G. Hennig^{6,7}, Ellad B. Tadmor⁸, Stefano Martiniani^{1,2,9,10*}**

¹Center for Soft Matter Research, Department of Physics,
 New York University, New York, NY 10003, USA

²Simons Center for Computational Physical Chemistry, Department of Chemistry,
 New York University, New York, NY 10003, USA

³Department of Computer Science & Engineering,
 University of Minnesota, Minneapolis, MN 55455, USA

⁴Department of Physics & Astronomy,
 Brigham Young University, Provo, UT 84602, USA

⁵Department of Chemistry,
 University of Florida, Gainesville, FL 32611, USA

⁶Quantum Theory Project,
 University of Florida, Gainesville, FL 32611, USA

⁷Department of Materials Science & Engineering,
 University of Florida, Gainesville, FL 32611, USA

⁸Department of Aerospace Engineering & Mechanics,
 University of Minnesota, Minneapolis, MN 55455, USA

⁹Center for Neural Science,
 New York University, New York, NY 10003, USA

¹⁰Courant Institute of Mathematical Sciences,
 New York University, New York, NY 10003, USA

Abstract

Generative models for materials, especially inorganic crystals, hold potential to transform the theoretical prediction of novel compounds and structures. Advancement in this field depends critically on robust benchmarks and minimal, information-rich datasets that enable meaningful model evaluation. This paper critically examines common datasets and reported metrics for a crystal structure prediction task—generating the most likely structures given the chemical composition of a material. We focus on three key issues: First, materials datasets should contain unique crystal structures; for example, we show that the widely-utilized *carbon-24* dataset only contains $\approx 40\%$ unique structures. Second, materials datasets should not be split randomly if polymorphs of many different compositions are numerous, which we find to be the case for the *perov-5* and *MP-20* datasets. Third, benchmarks can mislead if used uncritically, e.g., reporting a match rate metric without considering the structural variety exhibited by identical building blocks. To address these oft-overlooked issues, we introduce several fixes. We provide revised versions of the *carbon-24* dataset: one with duplicates removed, one deduplicated and split by number of atoms N , one with enantiomorphs, and two containing only identical structures but with different unit cells. We also propose new splits for datasets with polymorphs, ensuring that polymorphs are grouped within each split subset, setting a more sensible standard for benchmarking model performance. Finally, we present *METRe* and *cRMSE*, new model evaluation metrics that can correct existing issues with the match rate metric.

*Corresponding author: sm7683@nyu.edu.

1 Introduction

Recent advances in machine learning (ML) have fueled enormous interest in its application to materials science. For instance, machine-learning interatomic potentials have enabled efficient molecular simulations at near density-functional theory (DFT)-level accuracy [1, 2]. ML has also been applied to experiment planning and reaction prediction, enabling autonomous decision making in the laboratory through planning agents [3, 4]. This work concerns generative models for inorganic crystal structures, which learn mappings from a tractable base distribution to novel structures and compositions resembling the training data. This field has recently gained momentum, with numerous frameworks and architectures regularly claiming state-of-the-art performance [5–21].

The availability of high-quality and diverse datasets is paramount in the training and benchmarking of generative models. Minimal test datasets provide fast feedback during the development of generative models, prior to expensive training on large datasets. The bulk of materials datasets for the explicit purpose of materials discovery are generated using random structure searches with DFT [22, 23]. However, the influence of polymorphs (*i.e.*, different crystal structures for the same chemical compound) and structural duplicates in such standard datasets for inorganic crystal generation (see Fig. 1a–d), especially in the smallest test datasets, has largely been overlooked.

In addition to the datasets, the benchmark metrics themselves must be adequate to validate the quality of the generated samples and, therefore, to judge and compare different generative models [24, 25]. For the crystal-structure prediction (CSP) task—in which a generative model attempts to generate the positions and lattice vectors for a given composition—the match-rate metric is well established and thus reported in most works [5, 7–9, 12–16, 21, 26–28]. As we will discuss, however, the structure-matching procedure underlying this metric has limitations that must be overcome (see Fig. 1e).

In our paper, we demonstrate several examples where datasets and benchmarks have not been generated with the underlying scientific questions in mind. We elucidate the presence of a significant fraction of duplicate structures in the *carbon-24* dataset, the presence of polymorphic pairs of crystals with the same composition but different structure split randomly across the *perov-5* dataset(s), and benchmarking with match rates which lose meaning in the presence of polymorphs. We propose solutions through the publication of new datasets and dataset splits in addition to new benchmarks for assessing CSP task performance. We provide a brief crystallography primer with background on crystal-structure representations in Appendix F.

2 Related work

2.1 Crystal structure prediction and polymorphism

Crystal structure prediction aims to predict stable phases from a given composition. Polymorphs are distinct crystalline phases for the same chemical composition and are plentiful in the realm of experimental structural synthesis. Famously, inorganic compounds such as calcium carbonate can nucleate and grow in the aragonite, calcite, and vaterite crystalline phases [29]. Other well-known cases include carbon and its many allotropes—such as diamond, graphene, graphite, and buckminsterfullerene (buckyballs)—as well as silicon—which at both ambient condition and under pressure forms a large number of crystal phases [30, 31]. For molecular crystals, polymorphism is already well-understood to be the chief difficulty for CSP due to small free energy differences between stable polymorphs [32–34] which are pertinent to synthesis and drug design [35]. Even non-crystalline systems such as metamorphic proteins can adopt different stable, folded structures [36].

Thus, structure prediction from composition in generative models should thus consider the propensity to form various possible structural phases *from the same building blocks*. Although the standard datasets for CSP of atomic crystals contain polymorphs (as, *e.g.*, by design in the *carbon-24* dataset of carbon structures), their influence on performance metrics was previously not studied explicitly.

2.2 Existing datasets

In the literature, generative CSP models have been trained on very few datasets which have become the standard in the materials science domain. This paper is mainly concerned with three of them. The ***carbon-24*** dataset contains 10 153 structures consisting purely of carbon and containing up to

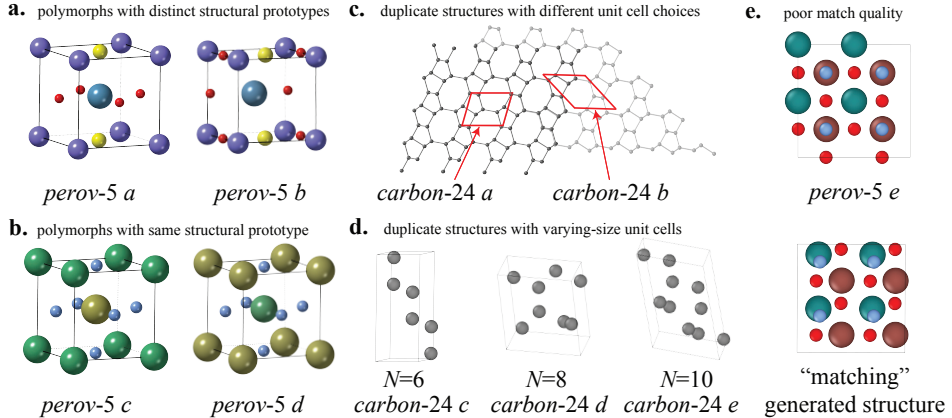


Figure 1: Enumerating existing features of datasets and benchmarks used in crystal structure prediction for generative models of inorganic crystals. (a) Two *perov-5* structures of composition CaCdSO_2 , but with different structural prototypes in which structure *b* is a distorted version of structure *a*. (b) Two *perov-5* structures of composition HfNbN_3 , with the same structural prototype but with the elements at the A and B sites (Hf and Nb) swapped in the perovskite ABX_3 structural prototype. (c) Two *carbon-24* duplicate structures (one in dark and the other in light gray) with their unit cells marked in red. (d) Three *carbon-24* duplicate structures with different unit cell sizes. (e) Views along a lattice direction of (top) a *perov-5* test set structure and (bottom) a structure from a generative model which are considered “matching” despite significant structural distortions between the two, calculated using Pymatgen’s `StructureMatcher` module with standard tolerances `ltol`= 0.3, `stol`= 0.5, `angle_tol`= 10.0.

24 atoms in the unit cell¹ [15]. It was curated from a ten-times larger dataset of carbon structures obtained at a pressure of 10 GPa in an *ab initio* random structure search [37] by choosing the structures with the lowest energy per atom. The *perov-5* dataset contains 18 928 perovskite structures [38]. Here, each unit cell contains five atoms with varying cell sizes (all cubic in shape) and chemical compositions. The *MP-20* dataset contains 45 229 structures from the Materials Project with up to 20 atoms per unit cell spanning a diverse range of unit cell shapes and compositions [15, 39].

The comparatively small *carbon-24* and *perov-5* datasets could, in principle, serve as minimal datasets with low computational cost during training and benchmarking. However, as we will discuss in Section 3, they contain duplicate structures and polymorphs that may result in misleading performance metrics. The *MP-20* dataset does not suffer as severely from these problems. Thoughtful benchmarks for *de novo* generation (DNG) from models trained on *MP-20* [40] are actively being expanded, while benchmarks for crystal structure prediction lag behind—even though good CSP models can be utilized for DNG if provided with novel compositions [5, 41].

2.3 Existing metrics

Benchmarking generative models for inorganic crystal structure prediction involves generating a structure for every composition in a test set. A typically reported metric is the **match rate** computed using Pymatgen’s `StructureMatcher` module [42] which performs a one-to-one comparison between the generated and reference structure. Here, the structures have to “match” only to some tolerance determined by the `stol`, `ltol`, and `angle_tol` parameters of the `StructureMatcher`: `stol` restricts how great the discrepancy between two sets of atomic sites can be, normalized by the average free length per atom $\sqrt[3]{V/N}$ where V is the volume of the (matched) unit cell and N is the number of atoms; `ltol` defines the fraction by which unit cell lengths are allowed to differ; `angle_tol` provides a bound on the difference in angle between matched unit cell vectors [42]. The alignment of two approximately matching structures is computed by an algorithm which reduces structures to their primitive cells, aligns lattice vectors within `ltol` tolerance, changes the basis of lattice vectors from one structure’s to the other’s—giving access to the (normalized) root-mean square error between the atom positions between two structures. This typically reported metric is the mean

¹A unit cell is a periodic building block that tiles space to form a crystalline material (see Appendix F).

RMSE, that is, the per-particle average root-mean-square error between matched generated and test structures. Non-matching structures are ignored for the computation of the mean RMSE.

For the *carbon*-24 dataset that consists entirely of different structures of the same composition, the match-rate metric is naturally ill-defined because of its one-to-many nature [5, 9, 12]. Some works alternatively report a k -match rate [8, 9, 12, 14, 28], where $k = 20$ structures are generated for every given composition in the test set. If at least one of the k generated structures matches the reference structure, the lowest-RMSE match is counted—thus k match rate considers possible polymorphs of crystals of the same composition in a statistical manner. If the generative model is able to generate several stable polymorphs (as desired), only one of the k trials has to yield a structure matching the specific structure in the test set in order to obtain a high k -match rate. However, evaluation of the k -match rate comes at a significantly higher computational cost, and k would need to be scaled with the expected number of polymorphs in the training data. An additional discussion of the k -match rate in comparison to the proposed metric of this paper is provided in Appendix A.1.

Thermodynamic (meta-)stability of generated structures (*i.e.*, having a negative or small energy above the convex hull of known stable structures) is an established metric for the *de novo* generation task of generative models for inorganic crystals [5, 6, 9–12, 20], where the model predicts both structure and composition. However, this is not a feasible metric for the *carbon*-24 and *perov*-5 datasets that include metastable structures by design [15, 37, 38]. For example, diamond is expected to be the only thermodynamically stable structure in the *carbon*-24 dataset.

2.4 Generative Models

In this work, we evaluate the performance of three generative models on various versions of the datasets introduced in Section 3. They perform either diffusion modeling [43, 44] or flow-based generative modeling [45, 46]—two major generative modeling paradigms. The first model, **DiffCSP** [14], is an equivariant diffusion model while the second one, **FlowMM** [12], is a flow-based generative model that applies the conditional flow matching framework [47]. The last model, **OMatG** [5], is a flow-based generative model which implements a general stochastic interpolant framework encompassing both diffusion modeling and conditional flow matching as special cases [45, 48].

3 Datasets

In this section, we discuss the deduplication (see Section 3.1) and polymorph-aware splitting (see Sections 3.2 and 3.3) of established datasets. We stress that no structural edits are made to individual crystals in this process: structures are either removed entirely, or regrouped into new splits. All new datasets can be found online at: <https://huggingface.co/collections/colabfit/datasets-all-that-structure-matches-does-not-glitter>.

3.1 Carbon structures

We show that the *carbon*-24 dataset contains far fewer unique structures than previously understood. An identification method for duplicates built upon Pymatgen’s **StructureMatcher** reveals that less than half of the 10 153 structures published in the dataset are, in fact, distinct. Consequently, we introduce two new variants: **carbon-24-unique** (see Section 3.1.1), which treats enantiomorphs² as duplicates, **carbon-24-unique-with-enantiomorphs** (see Section 3.1.2), which retains enantiomorphs as distinct structures, and the related toy dataset **carbon-enantiomorphs** with only the chiral pairs. The single-element nature of this data allows us to design additional benchmark datasets. We introduce the **carbon-24-unique- N -split** datasets (see Section 3.1.3), which make it possible to systematically study how well generative models can extrapolate beyond their training data to different unit cell sizes N . Finally, we explicitly use the identified duplicate structures to generate the **carbon-X** and **carbon-NXL** datasets for “overfitting” tests (see Section 3.1.4). We provide links to all of these datasets in Appendix B.

We note that our proposed identification method for duplicates based on the **StructureMatcher** can only provide highly *likely* duplicate candidates because it is still based on a limited numerical evaluation. Even defining a structure “match” is inherently ambiguous: Different settings can change

²Structures that are mirror images of each other but cannot be superimposed through translation or rotation.

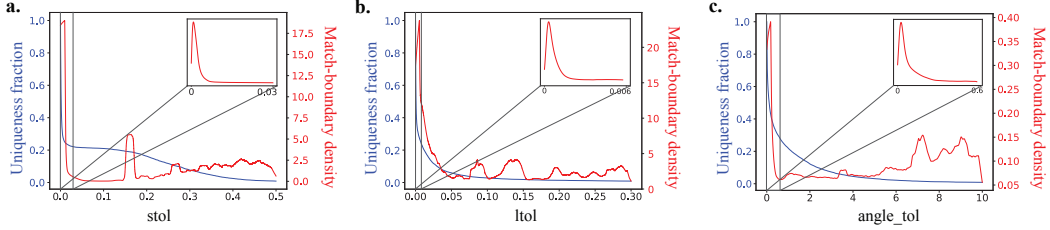


Figure 2: Kernel density estimates (with tophat kernel for large plots and Gaussian kernel for insets) of the distributions of match-boundary tolerance and uniqueness fraction for (a) `stol`, (b) `ltol`, and (c) `angle_tol` performed on the *carbon-24* dataset. These densities only count structure pairs which are considered matching at or below the maximum tolerances, and ignore structure pairs which are too structurally distinct to match.

whether two structures are considered matching or distinct. In dataset creation for generative models, we argue that the tolerance thresholds we set are sensible and informative given the current limits of CSP model performance.

3.1.1 Pruning duplicates

Pymatgen’s `StructureMatcher` has a variable tolerance for the comparison of two structures. The tolerances for the match-rate computation in the CSP task of generative models are generally chosen quite large (`stol`= 0.5, `ltol`= 0.3, and `angle_tol`= 10.0 which, in fact, exceed the default values of `stol`= 0.3, `ltol`= 0.2, and `angle_tol`= 5.0) [5, 7–9, 12–16, 21, 26–28]. Such loose tolerances may be reasonable when comparing imperfect structures obtained from generative models, which necessarily come with some uncertainty relative to the “perfect” crystals in the reference dataset, though their impact should still be carefully assessed (see Section 4.2). We note, however, that these tolerances are unsuitable for evaluating the structural distinctness within the *carbon-24* dataset itself.

In order to reasonably compare structures within *carbon-24*, we dynamically vary the tolerances of the `StructureMatcher`. For every pair of structures in the dataset, we find the match-boundary values of the `stol`, `ltol`, and `angle_tol` parameters where two structures transition from matching to non-matching. We use separate binary searches for every parameter while keeping the other ones fixed at their loose values `stol`= 0.5, `ltol`= 0.3, and `angle_tol`= 10.0. The `stol` parameter is not utilized in the alignment process; we make the simplifying approximation that the `ltol` and `angle_tol` tolerances can be treated independently. Further details on these computations is provided in Appendix J.

We show the distributions of the match-boundary tolerances for every tolerance parameter in Fig. 2. They all show signatures of a large peak at very low tolerance which is a clear sign of duplicate structures in the dataset. This is also confirmed by the estimated fraction of unique structures as a function of the tolerances in Fig. 2. This fraction reaches 1.0 only at very small values of the tolerance parameters. We conclude that the structure pairs within the peak at low tolerances represent replicated crystal structures that were not previously identified. The unit cells in the dataset can thus only be deemed all “distinct” if symmetries that leave the crystal structure unchanged are ignored. Unit cells, however, are *non-unique* representations of crystal structures, and an infinite number of choices of repeating units can be made which tile space to produce the crystal structure of interest (see Fig. 1c and d).

From Fig. 2, we estimate threshold values for each tolerance parameter below which the large peaks, indicative of duplicates structures, appear (`stol`= 0.025, `ltol`= 0.002, and `angle_tol`= 0.4). Using these thresholds, we generated three lists of duplicated structures (one for every tolerance parameter) that we combine into a single list by retaining only the pairs that appear in all three of them. After grouping the pairs into clusters, treating duplicates as mutual, we create a novel *carbon-24-unique* dataset by selecting a single representative from each cluster. This conservative cut leaves 4250 structures (down from 10 153) from which we create training, validation, and test sets with a random 60–20–20 % split.

3.1.2 Enantiomorph pairs

Certain chiral structures form enantiomorph pairs, mirror images that cannot be superimposed by any combination of proper rotations or translation.³ We noticed that chiral enantiomorph pairs were being tagged as duplicate structures by Pymatgen’s `StructureMatcher` since it allows for improper rotations (such as mirrors or inversions) in order to map two structures to one another. To identify enantiomorph pairs we disabled improper rotation mappings in `StructureMatcher` and recomputed the RMSE for all previously identified duplicate pairs. Pairs exhibiting a tenfold or greater increase in RMSE under this constraint were reclassified as enantiomorphs rather than duplicates.

We release the *carbon-24-unique-with-enantiomorphs* dataset which retains both structures in each enantiomorph pair and explicitly labels them. We found 80 enantiomorph pairs; we note that this screening was only applied to the structures in the *carbon-24-unique* dataset. We benchmark performance of models trained on one of each chiral pair in *carbon-enantiomorphs* (see H.3).

3.1.3 Datasets split by N

The single-element nature of the *carbon-24-unique* dataset provides a unique opportunity to isolate the effect of increasing size and structural complexity with the number of carbon atoms N . We thus introduce *carbon-24-unique- N -split* datasets, comprising non-random splits of the *carbon-24-unique* dataset that are organized by N . Structures are grouped into training, validation, and test sets by increasing (low-to-high) or decreasing (high-to-low) N , aiming for as close to a 60–20–20 % split as allowed by the groupings of N . For the low-to-high split, the training set contains 2280 structures with $N = 6$ –10 atoms, the validation set contains 1159 structures with $N = 12$ –14, and the test set contains 811 structures with $N = 16$ –24. Vice versa, for the high-to-low split, the training set contains 2633 structures with $N = 10$ –24, the validation set contains 792 structures with $N = 8$, and the test set contains 825 structures with $N = 6$.

Organizing the data by N allows us to systematically study how generative models generalize across different scales. This is also consequential for dataset creation, as smaller unit cells are significantly less expensive to obtain with DFT. Beyond carbon, such extrapolation is essential for modeling realistic materials systems that exhibit chemical or structural disorder, large unit cells, or even molecular motifs as in molecular crystals.

3.1.4 Datasets of duplicates

Pruning the *carbon-24* dataset of duplicates provides the opportunity to create datasets in which all crystals are identical to one another but with different choices of unit cells. From identified duplicate pairs, we publish and benchmark the use of two such datasets for use in “overfitting” tests for generative models. The first is the *carbon-X* dataset, which contains 480 carbon duplicate structures which have the same number of atoms N and cell shape L but different translations of the fractional coordinates X . The second is the *carbon-NXL* dataset, which contains 353 carbon duplicate structures that have different numbers of atoms per unit cell ($N = 6$ –16), different cell shapes L and fractional coordinates X (see Fig. 1c and d). As these two datasets each contain only a single structure and can be used to test whether the model can generate that singular structure, the datasets are not split.

These duplicate datasets are special because they are augmented with respect to an important type of symmetry—the equivalence of different unit cell choices for the same crystal—which standard encoders such as CSPNet [14] are not equivariant with respect to. CSPNet and the MatterGen model encoder [6] break invariance to this symmetry by injecting information about the lattice vectors or angles into their graph representations.

3.2 Polymorph-aware splits for perovskite structures

Unlike the *carbon-24* dataset, the *perov-5* dataset does not contain duplicates. It does, however, contain 9282 polymorph pairs (totaling 18 564 structures) and only 364 compositions that show up once in the dataset. These pairs are structurally dissimilar with either structural distortions (as in Fig. 1a) or elements swapped (as in Fig. 1b).

³A real-world example of a chiral pair of objects are human hands.

The full dataset was randomly split in a 60–20–20 % fashion by Xie et al. [15] into training, validation, and test sets, which raises the question: How are the structures in each polymorph pair distributed? There are 2265 composition matches between the validation and training set (out of 3787 validation set structures) and 2214 composition matches between the test and training set (out of 3785 test set structures). Only 94 validation set structures and 107 test set structures are considered “matching” with high RMSEs of ≈ 0.4 –0.5 to those in the training set, confirming high structural dissimilarity between the composition-matched structures. The random split of polymorph pairs into training, validation, and test sets implies that generative models are trained on one set of structures—and subsequently evaluated on their ability to generate a different structure of the same composition. We argue that this is a poor benchmark: even with a perfect model, it would be highly improbable that the precise structure in the test set be the one that is generated.

We publish and benchmark new splits for the *perov-5* dataset that we call ***perov-5-polymorph-split***, which confine polymorph pairs to be in the same portion of the split. For the evaluation over the validation and test sets, generative models will thus have to attempt to generate both structurally distinct structures of entirely unseen compositions. Under the assumption that a refined match-rate metric can handle polymorphs (see Section 4.1), this is arguably both a more reasonable task—with expectations for out-of-distribution generation adjusted—but also a harder task—generating multiple structures per composition for entirely new compounds—for benchmarking.

3.3 Polymorph-aware splits for large, diverse datasets

The *MP-20* dataset also contains polymorphs: 37 217 unique reduced compositions across 45 229 total structures ($\sim 82\%$ unique compositions). In contrast to the *perov-5* dataset, however, the fraction of non-unique compositions is much smaller. We provide new polymorph-aware splits *MP-20* dataset, termed ***MP-20-polymorph-split***. Unlike for the resplitting of the *perov-5* dataset, we consider how the propensity for a given composition to exhibit polymorphism could exhibit dependence on the number of unique elements of the material (commonly termed *n*-arity). In creating new splits for *MP-20*, polymorphs of the same composition were assigned to the same split, and the polymorphs groups were distributed such that the distribution of the *n*-arity of the combined dataset matched that of each individual split.

4 Benchmarking CSP model performance

4.1 Amending benchmarks to be robust to polymorphs

Datasets with many polymorphs, like the *carbon-24* and *perov-5* datasets, break the typically reported match-rate metric. Even if a generative model could produce all polymorphs of a given composition, it would score poorly because match-rate evaluates each generated structure against only one reference structure with the same composition. This one-to-one approach forces models to “learn” a unique structure per composition, ignoring the true multiplicity of (meta-)stable polymorphs and introducing an incorrect physical assumption.

We introduce the *match everyone to reference* (**METRe**) metric—pronounced ‘mēt-ər, like the SI unit—to assess how well generated structures cover the test set. Unlike standard match rate, METRe compares every reference structure against every generated (“match everyone”) and counts a match whenever a generated structure falls within tolerance of the reference structure (“to reference”), selecting only the best match per reference when computing the RMSE, as shown in Fig. 3a–e. The METRe rate is then the fraction of reference structures that find at least one match.

Counting “matches to everyone” with respect to generated structures is counterproductive because a model could have a high-scoring match metric by generating structures that resemble only a small fraction of reference structures. By contrast, METRe “matches to everyone” with respect to reference structures and does not have this issue. For datasets with many polymorphs (such as *carbon-24*), the ability to reproduce this structural diversity is essential, and METRe naturally accounts for it and rewards this behavior by counting matches with respect to the reference (test) set. In the limit of no polymorphism, the METRe rate reduces to the original definition of the match rate. In addition to the METRe metric, the mean RMSE and cRMSE (introduced in Section 4.2) between every reference structure and the best matching generated structure, as shown in Fig. 3, is equally if not more important. We provide Python code for the computation of the METRe and the cRMSE scores in Appendix A.

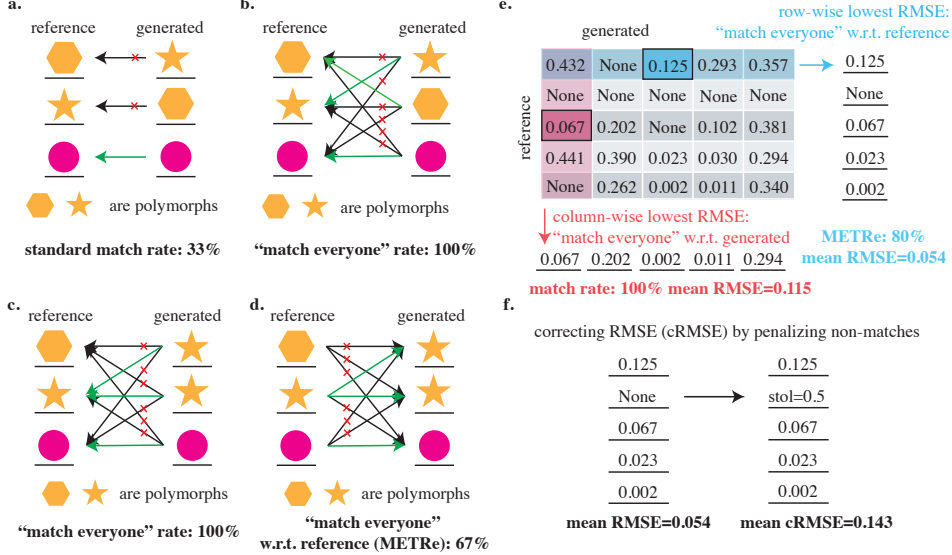


Figure 3: Demonstrating prior and new benchmarks. (a–d) A toy-case, in which the same colored shapes are considered polymorphs, shows different ways of computing match rate: (a) standard match rate, which penalizes polymorphs in the generated set being out of order; (b) “match everyone” metric, which fixes the fictitious penalty in (a); (c) a case of the “match everyone” metric in which a high match rate can be achieved without generating the diversity of polymorph structures; (d) our solution to the problems posed in (a) and (c), in which the number of matches from the “match everyone” metric is counted with respect to the reference set. (e) A demonstration of how “match everyone” differs when computed with respect to the generated vs. reference structures, showing that only the metric with respect to the reference structures (METRe) catches cases in which none of the generated structures match a given reference structure. (f) The implementation of corrected RMSE on a given matching metric.

We emphasize that the k -match rate (see Section 2.3) is fundamentally different from the METRe rate as the latter is measuring matches with respect to the entire test set. In future work, one could consider an analogous k -METRe rate where the generated set is larger than the reference set thus mitigating the effect of statistical fluctuations in the generation of different polymorph structures. We add as a final note that METRe becomes inflated and harder to interpret correctly if there are many duplicates in the test set—which is undesirable in the context of generative modeling—and therefore duplicate structures should be removed from the dataset before using the METRe rate.

4.2 New metric to combine RMSE and match rate

Optimizing generative models only with respect to match or METRe rates, say in a hyperparameter sweep, may lead to models that poorly match to a large number of the test set structures (see Fig. 1e where two structures with little structural similarity are considered matching). The application of `StructureMatcher` to compute structure matches is highly tolerant—for example, usage with standard tolerances to compute matches would suggest that the uniqueness rate within the *carbon-24* dataset (see Fig. 2) is between 3–4 %. Thus, METRe alone is not a sufficiently strong metric for optimizing generative models for crystalline materials. Similarly, the mean RMSE metric alone is also insufficiently qualitative because the RMSE between two structures is only computed if structures are matched. In the worst case, models may learn to generate only a single structure from the test set to high accuracy. Compatible with this discussion, we note that the recent work on the OMatG model observed an apparent tradeoff between the match-rate metric and the mean RMSE [5].

We propose a new corrected RMSE (**cRMSE**) metric that combines the METRe and RMSE metrics, as illustrated in Fig. 3e. We define cRMSE by penalizing non-matching structures by using `stol` as the non-matching RMSE (instead of ignoring the missing match). We choose `stol` as the penalty because it sets the threshold for the computed RMSE of the aligned structures in `StructureMatcher` (if a mapping can be found).

Table 1: Benchmarking generative models (OMatG labeled by positional interpolant) on the new *carbon*-24-unique and *perov*-5-polymorph-split datasets, as well as the original *perov*-5 datasets using the proposed METRe match rate, mean RMSE, and corrected mean cRMSE metrics. For the *carbon*-24-unique generated structures, we also report the result of standard match rate and corresponding RMSE for comparison.*

Model	<i>carbon</i> -24-unique			<i>perov</i> -5			<i>perov</i> -5-polymorph-split		
	Std. Match % (\uparrow) / RMSE (\downarrow)	METRe % (\uparrow) / RMSE (\downarrow) / cRMSE (\downarrow)	METRe % (\uparrow) / RMSE (\downarrow) / cRMSE (\downarrow)	METRe % (\uparrow) / RMSE (\downarrow) / cRMSE (\downarrow)	METRe % (\uparrow) / RMSE (\downarrow) / cRMSE (\downarrow)	METRe % (\uparrow) / RMSE (\downarrow) / cRMSE (\downarrow)			
DiffCSP*	21.2 % / 0.380	98.2 % / 0.231 / 0.235	57.7 % / 0.072 / 0.253	78.9 % / 0.072 / 0.162					
FlowMM*	19.5 % / 0.358	98.4 % / 0.193 / 0.198	58.4 % / 0.096 / 0.264	78.8 % / 0.070 / 0.161					
OMatG-LinearODE	19.8 % / 0.286	98.0 % / 0.183 / 0.189	67.5 % / 0.236 / 0.322	76.8 % / 0.055 / 0.158					
OMatG-LinearODE γ	16.9 % / 0.314	97.6 % / 0.213 / 0.220	76.3 % / 0.344 / 0.381	75.9 % / 0.067 / 0.172					
OMatG-TrigODE	18.8 % / 0.272	98.5 % / 0.183 / 0.187	84.3 % / 0.359 / 0.381	77.1 % / 0.059 / 0.160					
OMatG-TrigODE γ	19.8 % / 0.307	98.1 % / 0.181 / 0.187	75.7 % / 0.313 / 0.358	76.3 % / 0.053 / 0.159					
OMatG-EncDecODE	18.1 % / 0.298	98.2 % / 0.195 / 0.201	72.6 % / 0.398 / 0.425	74.5 % / 0.058 / 0.171					
OMatG-SBDODE	14.8 % / 0.324	97.8 % / 0.218 / 0.224	85.1 % / 0.366 / 0.386	77.1 % / 0.062 / 0.163					

*Starred model names have identical hyperparameters for both *perov*-5 splits. OMatG models were hyperparameter tuned for maximizing standard match rate on *perov*-5 and minimizing cRMSE on *perov*-5-polymorph-split.

For a mathematical definition of the mean cRMSE metric, let N_{test} be the number of test set structures, $N_{\text{ref.match}}$ the number of matches according to the METRe metric, and RMSE_i the relevant RMSE for the i th structure in the test set. We can then express the mean cRMSE as

$$\begin{aligned} \text{mean cRMSE(stol)} &= \frac{\sum_{i=1}^{N_{\text{ref.match}}} \text{RMSE}_i + \text{stol}(N_{\text{test}} - N_{\text{ref.match}})}{N_{\text{test}}} \\ &= \text{METRe} * (\text{mean RMSE} - \text{stol}) + \text{stol}, \end{aligned} \quad (1)$$

where we used $\text{METRe} = N_{\text{ref.match}}/N_{\text{test}}$ and $\text{mean RMSE} = \sum_{i=1}^{N_{\text{ref.match}}} \text{RMSE}_i/N_{\text{ref.match}}$.

We note that the cRMSE metric can also be defined with the original definition of the match-rate metric. It is a general way to combine any match-rate metric with an RMSE for the optimization of generative models. We also emphasize that mean cRMSE can be rewritten as a combination of any type of match rate and corresponding mean RMSE as a function of the `stol` used with `StructureMatcher`. We propose that the **primary benchmark for CSP performance should be the mean cRMSE(stol)** instead of the match or METRe rate and RMSE separately.

5 Results

We benchmark DiffCSP, FlowMM, and OMatG on our new datasets using METRe and cRMSE, with cRMSE as the primary performance metric, using the standard `stol= 0.5`, `1tol= 0.3`, `angle_tol= 10.0` for `StructureMatcher`. This means that all reported cRMSE values are a function of `stol = 0.5`. Hyperparameter choices (using published ones for DiffCSP and FlowMM) and optimization (hyperparameter tuning for lower cRMSE for OMatG) are discussed in Appendix D. The flexibility of OMatG allows us to study a wide variety of models that are differentiated by the choice of a positional interpolant (for more details, see Ref. [5]). We further note that all of the standard match rates and METRe results are reported without any filtering for structural or compositional validity (as in Ref. [5]). The filtering is not necessary as high RMSE or cRMSE values will indicate poor quality of matches with greater propensity for structural invalidity. We also report our new benchmarks on old datasets: for *perov*-5 (see Table 1) and *MP*-20 (see Table 2).

In Table 1, we compare the performance of the models on the *carbon*-24-unique and *perov*-5-polymorph-split datasets. We also include results for the original *perov*-5 dataset split for comparison. For the *carbon*-24-unique dataset, we measure the performance on identical generated structures with both standard match (one-to-one) and METRe rates and highlight the significant jump in fraction of matches identified by accounting for polymorphism. Comparing the RMSE values between standard matching and METRe, we also note a ≈ 0.1 decrease in the average RMSE for matching structures. Finally, for METRe we also compute the cRMSE, which is close to the RMSE values since the METRe value is high. Overall for the *carbon*-24-unique dataset, the METRe rate and its corresponding RMSE and cRMSE values indicate the strongest performance for trigonometric positional interpolants using OMatG, followed closely by the performance for linear flow-matching with both OMatG and FlowMM.

Table 2: Benchmarking generative models on the *MP*-20 and *MP*-20-polymorph-split datasets using the proposed METRe match rate, mean RMSE, and corrected mean cRMSE metrics. DiffCSP and FlowMM models both use published *MP*-20 hyperparameters (consistent across the two datasets, signified by the * next to the model name). The OMatG model was hyperparameter tuned to optimize for high match rate on *MP*-20 and low cRMSE on the *MP*-20-polymorph-split dataset.

Model	<i>MP</i> -20			<i>MP</i> -20-polymorph-split		
	METRe % (\uparrow)	RMSE (\downarrow)	cRMSE (\downarrow)	METRe % (\uparrow)	RMSE (\downarrow)	cRMSE (\downarrow)
DiffCSP*	58.8 %	0.064	0.244	53.1 %	0.084	0.279
FlowMM*	67.0 %	0.067	0.210	65.2 %	0.079	0.226
OMatG-LinearODE	66.0 %	0.058	0.208	70.5 %	0.056	0.187

For the *perov*-5-polymorph-split dataset, we assess the models’ performances using METRe, RMSE and cRMSE, and compare the results to those obtained for models trained on the *perov*-5 split. Arguably, the *perov*-5-polymorph-split is a challenging objective because the model is expected to produce two structures (recall that each composition admits two polymorphs in this dataset) from compositions that it has never encountered. Nevertheless, the model performance on the *perov*-5-polymorph-split dataset is improved relative to the previous *perov*-5 dataset across most METRe rates and all METRe-associated RMSE and cRMSE values. Again, the strongest performance in terms of RMSE and cRMSE is obtained for linear and trigonometric interpolant OMatG models, while the strongest performance for METRe was for DiffCSP; differences in cRMSE, however, are modest between all models. These results suggest that by simply splitting the *perov*-5 data differently, the models are better able to generalize not only to new compositions but also to new structural prototypes.

For the *MP*-20-polymorph-split dataset, we include in Table 2 results for the METRe, RMSE, and cRMSE metrics for models trained on the previous (*MP*-20) and the new (*MP*-20-polymorph-split) dataset splits. Structures for the DiffCSP and FlowMM models were generated using published *MP*-20 hyperparameters. For DiffCSP and FlowMM, performance on the polymorph-aware dataset split declined in comparison to the original dataset split. This is unsurprising given that the hyperparameters were tuned without polymorph-aware benchmarks on the original dataset split. For OMatG models—through a hyperparameter optimization procedure for both dataset splits—we observed a modest improvement in performance and higher state-of-the-art performance metrics.

We also benchmark on the “duplicates” datasets and show results in Table 3 for *carbon*-*NXL* and in Table 4 in Appendix H.1 for *carbon*-*X*. For these datasets, we restrict benchmarks to only the OMatG conditional flow-matching model (OMatG-Linear) and compare results for the standard CSPNet encoder to an augmented CSPNet—which adds both lattice angle information as well as the number of atoms N to the representation. We report the standard match rate for these benchmarks, because the test set (*i.e.*, the training set) contains only a single crystal structure. For the *carbon*-*NXL* dataset, we additionally benchmark the models by isolating reported metrics by N , pinpointing the difficulty of generating identical structures with more atoms. These datasets provide idealized conditions in which no compositional complexity and exactly one structural prototype needs to be learned by the model, and difficulty of the task can be controlled systematically by varying N .

Performance deteriorates for the *carbon*-*NXL* dataset as the number of atoms N and lattice vectors L change, with only 60–69% match rate for structures with $N = 6$ and significantly lower match rates of 26–39% for $N = 8$, along with RMSE values an order of magnitude higher (Table 3). To our knowledge, this is the first study for inorganic crystals to provably demonstrate that performance is limited not just by structural or compositional complexity, but also by the dimensionality of the learned flows as defined by the unit-cell size N .

To further examine the impact of N , we use the hyperparameters from models trained on the *carbon*-24-unique dataset and report METRe, RMSE, and cRMSE in Table 5 in Appendix H.1 for models trained on the *carbon*-24-unique- N -split datasets. Comparing the low-to-high to the high-to-low N -split, we find that the latter yields significantly better results. This is to be expected: we already demonstrated that low- N structures are considerably better at achieving high-fidelity matches. The low-to-high N -split performs poorly and serves as a challenging objective for future generative models to target.

Table 3: Benchmarking the *carbon-NXL* duplicates dataset using mean RMSE, corrected mean cRMSE, and standard match rate (chosen because there is only one unique structure in the dataset). Training and generation initialization were both performed with the entire dataset. Results are reported for the complete dataset and broken down by unit cell size N . A conditional flow-matching OMatG-LinearODE model was used with two choices of encoders, CSPNet and augmented CSPNet with lattice angle and N information. We exclude metrics for $N = 10\text{--}16$ due to deficiency of such structures in both the train and test dataset and, thus, the unpredictability of the generated structures.

Model	<i>carbon-NXL</i>						$N = 8$		
	All N			$N = 6$					
	Std. Match (%) \uparrow	RMSE \downarrow	cRMSE \downarrow	Std. Match (%) \uparrow	RMSE \downarrow	cRMSE \downarrow	Std. Match (%) \uparrow	RMSE \downarrow	cRMSE \downarrow
CSPNet	47.3 %	0.008	0.266	60.0 %	0.005	0.203	39.0 %	0.013	0.310
aug-CSPNet	47.7 %	0.006	0.264	69.2 %	0.005	0.157	26.0 %	0.010	0.373

6 Discussion

We have shown that progress demands not only advanced generative models but also meticulously curated, task-aligned datasets and evaluation metrics designed for the specific challenges within crystal structure prediction. By systematically analyzing widely-used benchmarks for CSP, we uncover ill-posed assessments and improperly curated datasets. To rectify these issues, we introduced new curated datasets and dataset splits and benchmarks that expand the scope of evaluating CSP performance. Our results demonstrate that improved dataset design and evaluation criteria lead to better performance on more difficult tasks. Our analysis also revealed that the performance of generative models degrades with unit-cell size N , elucidating a clear challenge for generative models. We hope that our datasets, metrics and benchmarks will contribute to the foundation of this field, encouraging more rigorous practices in model evaluation and dataset design.

Acknowledgments and Disclosure of Funding

The authors would like to thank Shenglong Wang at NYU IT HPC and Gregory Wolfe for their support in this work. The authors acknowledge funding from NSF Grant OAC-2311632. P. H. and S. M. also acknowledge support from the Simons Center for Computational Physical Chemistry (Simons Foundation grant 839534, MT). The authors gratefully acknowledge the computational resources and consultation support that have contributed to the research results reported in this publication, provided by: IT High Performance Computing at New York University; the Empire AI Consortium; UFIT Research Computing and the NVIDIA AI Technology Center at the University of Florida in part through the AI and Complex Computational Research Award.

References

- [1] Ilyes Batatia, David P. Kovacs, Gregor Simm, Christoph Ortner, and Gabor Csanyi. MACE: Higher Order Equivariant Message Passing Neural Networks for Fast and Accurate Force Fields. *Advances in Neural Information Processing Systems*, 35:11423–11436, December 2022. URL <https://arxiv.org/abs/2206.07697>.
- [2] Simon Batzner, Albert Musaelian, Lixin Sun, Mario Geiger, Jonathan P. Mailoa, Mordechai Kornbluth, Nicola Molinari, Tess E. Smidt, and Boris Kozinsky. E(3)-equivariant graph neural networks for data-efficient and accurate interatomic potentials. *Nature Communications*, 13(1):2453, May 2022. ISSN 2041-1723. doi: 10.1038/s41467-022-29939-5. URL <https://www.nature.com/articles/s41467-022-29939-5>.
- [3] Daniil A. Boiko, Robert MacKnight, Ben Kline, and Gabe Gomes. Autonomous chemical research with large language models. *Nature*, 624(7992):570–578, December 2023. ISSN 0028-0836, 1476-4687. doi: 10.1038/s41586-023-06792-0.
- [4] Haorui Wang, Jeff Guo, Lingkai Kong, Rampi Ramprasad, Philippe Schwaller, Yuanqi Du, and Chao Zhang. LLM-Augmented Chemical Synthesis and Design Decision Programs, May 2025.
- [5] Philipp Höllmer, Thomas Egg, Maya M. Martirosyan, Eric Fuemmeler, Amit Gupta, Zeren Shui, Pawan Prakash, Adrian Roitberg, Mingjie Liu, George Karypis, Mark Transtrum, Richard G. Hennig, Ellad B. Tadmor, and Stefano Martiniani. Open materials generation with stochastic interpolants. In *Forty-second International Conference on Machine Learning*, 2025. URL <https://openreview.net/forum?id=egHGrzxFuJU>. Also at arXiv:2502.02582 (<https://arxiv.org/abs/2502.02582>).
- [6] Claudio Zeni, Robert Pinsler, Daniel Zügner, Andrew Fowler, Matthew Horton, Xiang Fu, Zilong Wang, Aliaksandra Shysheya, Jonathan Crabbé, Shoko Ueda, Roberto Sordillo, Lixin Sun, Jake Smith, Bichlien Nguyen, Hannes Schulz, Sarah Lewis, Chin-Wei Huang, Ziheng Lu, Yichi Zhou, Han Yang, Hongxia Hao, Jielan Li, Chunlei Yang, Wenjie Li, Ryota Tomioka, and Tian Xie. A generative model for inorganic materials design. *Nature*, January 2025. ISSN 0028-0836, 1476-4687. doi: 10.1038/s41586-025-08628-5.
- [7] Ziyi Chen, Yang Yuan, Siming Zheng, Jialong Guo, Sihan Liang, Yangang Wang, and Zongguo Wang. Transformer-Enhanced Variational Autoencoder for Crystal Structure Prediction, February 2025.
- [8] Yuji Tone, Masatoshi Hanai, Mitsuaki Kawamura, Kenjiro Taura, and Toyotaro Suzumura. ContinuouSP: Generative Model for Crystal Structure Prediction with Invariance and Continuity, February 2025.
- [9] François R J Cornet, Federico Bergamin, Arghya Bhownik, Juan Maria Garcia-Lastra, Jes Frellsen, and Mikkel N. Schmidt. Kinetic langevin diffusion for crystalline materials generation. In *AI for Accelerated Materials Design - ICLR 2025*, 2025. URL <https://openreview.net/forum?id=Mttf1RoKKM>.
- [10] Chaitanya K. Joshi, Xiang Fu, Yi-Lun Liao, Vahe Gharakhanyan, Benjamin Kurt Miller, Anuroop Sriram, and Zachary W. Ulissi. All-atom diffusion transformers: Unified generative modelling of molecules and materials, 2025. URL <https://arxiv.org/abs/2503.03965>.
- [11] Anuroop Sriram, Benjamin Kurt Miller, Ricky T. Q. Chen, and Brandon M. Wood. FlowLLM: Flow Matching for Material Generation with Large Language Models as Base Distributions, October 2024. URL <http://arxiv.org/abs/2410.23405>.
- [12] Benjamin Kurt Miller, Ricky T. Q. Chen, Anuroop Sriram, and Brandon M. Wood. FlowMM: Generating Materials with Riemannian Flow Matching, June 2024. URL <http://arxiv.org/abs/2406.04713>.
- [13] Rui Jiao, Wenbing Huang, Yu Liu, Deli Zhao, and Yang Liu. Space Group Constrained Crystal Generation, April 2024. URL <http://arxiv.org/abs/2402.03992>.

[14] Rui Jiao, Wenbing Huang, Peijia Lin, Jiaqi Han, Pin Chen, Yutong Lu, and Yang Liu. Crystal Structure Prediction by Joint Equivariant Diffusion, July 2023. URL <https://arxiv.org/abs/2309.04475v2>.

[15] Tian Xie, Xiang Fu, Octavian-Eugen Ganea, Regina Barzilay, and Tommi Jaakkola. Crystal Diffusion Variational Autoencoder for Periodic Material Generation, March 2022.

[16] Hanlin Wu, Yuxuan Song, Jingjing Gong, Ziyao Cao, Yawen Ouyang, Jianbing Zhang, Hao Zhou, Wei-Ying Ma, and Jingjing Liu. A Periodic Bayesian Flow for Material Generation, February 2025.

[17] Izumi Takahara, Kiyou Shibata, and Teruyasu Mizoguchi. Generative Inverse Design of Crystal Structures via Diffusion Models with Transformers, June 2024.

[18] Astrid Klipfel, Zied Bouraoui, Olivier Peltre, Yaël Fregier, Najwa Harrati, and Adlane Sayede. Equivariant Message Passing Neural Network for Crystal Material Discovery. *Proceedings of the AAAI Conference on Artificial Intelligence*, 37(12):14304–14311, June 2023. ISSN 2374-3468, 2159-5399. doi: 10.1609/aaai.v37i12.26673.

[19] Krit Tangsongcharoen, Teerachote Pakornchote, Chayanon Atthapak, Natthaphon Choomphon-anomakhun, Annop Ektarawong, Björn Alling, Christopher Sutton, Thiti Bovornratanarak, and Thiparat Chotibut. CrystalGRW: Generative Modeling of Crystal Structures with Targeted Properties via Geodesic Random Walks, March 2025.

[20] Subhojoyoti Khastagir, KISHALAY DAS, Pawan Goyal, Seung-Cheol Lee, Satadeep Bhattacharjee, and Niloy Ganguly. CrysLDM: Latent diffusion model for crystal material generation. In *AI for Accelerated Materials Design - ICLR 2025*, 2025. URL <https://openreview.net/forum?id=mhe4EejyAS>.

[21] Kishalay Das, Subhojoyoti Khastagir, Pawan Goyal, Seung-Cheol Lee, Satadeep Bhattacharjee, and Niloy Ganguly. Periodic Materials Generation using Text-Guided Joint Diffusion Model, March 2025.

[22] Chris J. Pickard and R. J. Needs. High-Pressure Phases of Silane. *Physical Review Letters*, 97(4):045504, July 2006. ISSN 0031-9007, 1079-7114. doi: 10.1103/PhysRevLett.97.045504. URL <https://link.aps.org/doi/10.1103/PhysRevLett.97.045504>.

[23] Chris J Pickard and R J Needs. *Ab Initio* random structure searching. *J. Phys.: Condens. Matter*, 23(5):053201, February 2011. ISSN 0953-8984, 1361-648X. doi: 10.1088/0953-8984/23/5/053201. URL <https://iopscience.iop.org/article/10.1088/0953-8984/23/5/053201>.

[24] Ahmed Alaa, Boris Van Breugel, Evgeny S. Saveliev, and Mihaela van der Schaar. How faithful is your synthetic data? Sample-level metrics for evaluating and auditing generative models. In Kamalika Chaudhuri, Stefanie Jegelka, Le Song, Csaba Szepesvari, Gang Niu, and Sivan Sabato, editors, *Proceedings of the 39th International Conference on Machine Learning*, volume 162 of *Proceedings of Machine Learning Research*, pages 290–306. PMLR, 17–23 Jul 2022. URL <https://proceedings.mlr.press/v162/ala22a.html>.

[25] Qiantong Xu, Gao Huang, Yang Yuan, Chuan Guo, Yu Sun, Felix Wu, and Kilian Weinberger. An empirical study on evaluation metrics of generative adversarial networks, August 2018.

[26] Yang Liu, Chuan Zhou, Shuai Zhang, Peng Zhang, Xixun Lin, and Shirui Pan. Equivariant Hypergraph Diffusion for Crystal Structure Prediction, January 2025.

[27] Rui Jiao, Xiangzhe Kong, Wenbing Huang, and Yang Liu. 3d structure prediction of atomic systems with flow-based direct preference optimization. In *The Thirty-eighth Annual Conference on Neural Information Processing Systems*, 2024. URL <https://openreview.net/forum?id=EpusilXfNd>.

[28] Luis M. Antunes, Keith T. Butler, and Ricardo Grau-Crespo. Crystal structure generation with autoregressive large language modeling. *Nature Communications*, 15(1):10570, December 2024. ISSN 2041-1723. doi: 10.1038/s41467-024-54639-7.

[29] M. Sudhakara Reddy. Biomineralization of calcium carbonates and their engineered applications: A review. *Frontiers in Microbiology*, 4, October 2013. ISSN 1664-302X. doi: 10.3389/fmicb.2013.00314. URL <https://www.frontiersin.org/journals/microbiology/articles/10.3389/fmicb.2013.00314/full>.

[30] R. G. Hennig, A. Wadehra, K. P. Driver, W. D. Parker, C. J. Umrigar, and J. W. Wilkins. Phase transformation in Si from semiconducting diamond to metallic β -Sn phase in QMC and DFT under hydrostatic and anisotropic stress. *Physical Review B*, 82(1):014101, July 2010. doi: 10.1103/PhysRevB.82.014101. URL <https://link.aps.org/doi/10.1103/PhysRevB.82.014101>.

[31] Eric B. Jones and Vladan Stevanović. Polymorphism in elemental silicon: Probabilistic interpretation of the realizability of metastable structures. *Physical Review B*, 96(18):184101, November 2017. doi: 10.1103/PhysRevB.96.184101. URL <https://link.aps.org/doi/10.1103/PhysRevB.96.184101>.

[32] Jonas Nyman and Graeme M. Day. Static and lattice vibrational energy differences between polymorphs. *CrystEngComm*, 17(28):5154–5165, July 2015. ISSN 1466-8033. doi: 10.1039/C5CE00045A.

[33] Sarah L. Price. Control and prediction of the organic solid state: A challenge to theory and experiment. *Proceedings. Mathematical, Physical, and Engineering Sciences*, 474(2217):20180351, September 2018. ISSN 1364-5021. doi: 10.1098/rspa.2018.0351. URL <https://www.ncbi.nlm.nih.gov/pmc/articles/PMC6189584/>.

[34] Nikolaos Galanakis and Mark E. Tuckerman. Rapid prediction of molecular crystal structures using simple topological and physical descriptors. *Nature Communications*, 15(1):9757, November 2024. ISSN 2041-1723. doi: 10.1038/s41467-024-53596-5.

[35] Dmitry Chistyakov and Gleb Sergeev. The Polymorphism of Drugs: New Approaches to the Synthesis of Nanostructured Polymorphs. *Pharmaceutics*, 12(1):34, January 2020. ISSN 1999-4923. doi: 10.3390/pharmaceutics12010034. URL <https://pmc.ncbi.nlm.nih.gov/articles/PMC7022426/>.

[36] Carlo Camilloni and Ludovico Sutto. Lymphotactin: How a protein can adopt two folds. *The Journal of Chemical Physics*, 131(24):245105, December 2009. ISSN 1089-7690. doi: 10.1063/1.3276284.

[37] Chris J. Pickard. AIRSS data for carbon at 10GPa and the C+N+H+O system at 1GPa, March 2020. URL <https://archive.materialscloud.org/record/2020.0026/v1>.

[38] Ivano E. Castelli, David D. Landis, Kristian S. Thygesen, Søren Dahl, Ib Chorkendorff, Thomas F. Jaramillo, and Karsten W. Jacobsen. New cubic perovskites for one- and two-photon water splitting using the computational materials repository. *Energy & Environmental Science*, 5(10):9034–9043, September 2012. ISSN 1754-5706. doi: 10.1039/C2EE22341D. URL <https://pubs.rsc.org/en/content/articlelanding/2012/ee/c2ee22341d>.

[39] Anubhav Jain, Shyue Ping Ong, Geoffroy Hautier, Wei Chen, William Davidson Richards, Stephen Dacek, Shreyas Cholia, Dan Gunter, David Skinner, Gerbrand Ceder, and Kristin A. Persson. Commentary: The Materials Project: A materials genome approach to accelerating materials innovation. *APL Materials*, 1(1):011002, July 2013. doi: 10.1063/1.4812323. URL <https://aip.scitation.org/doi/10.1063/1.4812323>.

[40] Nathan J. Szymanski and Christopher J. Bartel. Establishing baselines for generative discovery of inorganic crystals, January 2025. URL <http://arxiv.org/abs/2501.02144>.

[41] Amil Merchant, Simon Batzner, Samuel S. Schoenholz, Muratahan Aykol, Gowoon Cheon, and Ekin Dogus Cubuk. Scaling deep learning for materials discovery. *Nature*, 624:80–85, November 2023. ISSN 1476-4687. doi: 10.1038/s41586-023-06735-9. URL <https://www.nature.com/articles/s41586-023-06735-9>.

[42] Shyue Ping Ong, William Davidson Richards, Anubhav Jain, Geoffroy Hautier, Michael Kocher, Shreyas Cholia, Dan Gunter, Vincent L. Chevrier, Kristin A. Persson, and Gerbrand Ceder. Python Materials Genomics (pymatgen): A robust, open-source python library for materials analysis. *Computational Materials Science*, 68:314–319, February 2013. ISSN 0927-0256. doi: 10.1016/j.commatsci.2012.10.028. URL <https://www.sciencedirect.com/science/article/pii/S0927025612006295>.

[43] Jonathan Ho, Ajay Jain, and Pieter Abbeel. Denoising Diffusion Probabilistic Models, December 2020.

[44] Yang Song, Jascha Sohl-Dickstein, Diederik P. Kingma, Abhishek Kumar, Stefano Ermon, and Ben Poole. Score-Based Generative Modeling through Stochastic Differential Equations, February 2021. URL <http://arxiv.org/abs/2011.13456>.

[45] Michael S. Albergo, Nicholas M. Boffi, and Eric Vanden-Eijnden. Stochastic Interpolants: A Unifying Framework for Flows and Diffusions, November 2023. URL <http://arxiv.org/abs/2303.08797>.

[46] Yaron Lipman, Ricky T. Q. Chen, Heli Ben-Hamu, Maximilian Nickel, and Matt Le. Flow Matching for Generative Modeling, February 2023. URL <http://arxiv.org/abs/2210.02747>.

[47] Ricky T. Q. Chen and Yaron Lipman. Flow Matching on General Geometries, February 2024. URL <http://arxiv.org/abs/2302.03660>.

[48] Michael S. Albergo, Mark Goldstein, Nicholas M. Boffi, Rajesh Ranganath, and Eric Vanden-Eijnden. Stochastic interpolants with data-dependent couplings, September 2024. URL <http://arxiv.org/abs/2310.03725>.

[49] Jonathan Schmidt, Noah Hoffmann, Hai-Chen Wang, Pedro Borlido, Pedro J. M. A. Carriço, Tiago F. T. Cerqueira, Silvana Botti, and Miguel A. L. Marques. Large-scale machine-learning-assisted exploration of the whole materials space, October 2022. URL <http://arxiv.org/abs/2210.00579>.

[50] Jonathan Schmidt, Noah Hoffmann, Wang Hai-Chen, Pedro Borlido, Pedro J. M. A. Carriço, F. T. Cerqueira Tiago, Silvana Botti, and Miguel A. L. Marques. Large-scale machine-learning-assisted exploration of the whole materials space. 2022. doi: 10.24435/materialscloud:m7-50. URL <https://archive.materialscloud.org/records/hvq5r-dby55>.

[51] Richard Liaw, Eric Liang, Robert Nishihara, Philipp Moritz, Joseph E Gonzalez, and Ion Stoica. Tune: A research platform for distributed model selection and training. *arXiv preprint arXiv:1807.05118*, 2018.

[52] J. Bergstra, D. Yamins, and D. D. Cox. Making a Science of Model Search: Hyperparameter Optimization in Hundreds of Dimensions for Vision Architectures. *TProc. of the 30th International Conference on Machine Learning (ICML 2013)*, pages pp. I–115 to I–123, 2013.

[53] International Tables for Crystallography, Vol. A: Space-group Symmetry. Wiley, second online edition edition, 2016. URL <https://it-iucr-org.proxy.library.nyu.edu/Ac/>.

[54] R. W. Grosse-Kunstleve, N. K. Sauter, and P. D. Adams. Numerically stable algorithms for the computation of reduced unit cells. *Acta Cryst A*, 60(1):1–6, January 2004. ISSN 0108-7673. doi: 10.1107/S010876730302186X. URL <http://journals.iucr.org/paper?sh5006>.

[55] Atsushi Togo, Kohei Shinohara, and Isao Tanaka. Spglib: A software library for crystal symmetry search, March 2024. URL <http://arxiv.org/abs/1808.01590>.

A METRe and cRMSE metrics

The code for calculation of the METRe metric and mean cRMSE is available within the OMatG software hosted at <https://github.com/FERMat-ML/OMatG>.

A.1 Comparison to k -match rate

As discussed in Section 2.3, the k -match rate depends on a fixed integer value for k that determines the number of generated structure for each reference structure. If one of these k generated structures matches the reference structure, a match is recorded. This approach ameliorates the problem of polymorphism since the model has more opportunities to generate the correct polymorph under consideration. By scaling k , the probability of producing the reference polymorph increases. In order to assess whether the generative model is able to generate all possible polymorphs, k should be at least the number of maximum polymorphs in the dataset.

METRe possesses two key advantages over the k -match rate. First, METRe requires no explicit definition of k . Instead, METRe only requires as many generated structures as are present in the test dataset. As a result, METRe is more efficient at inference time. Second, METRe wastes no structure in that each generated structure is compared against each reference structure. It automatically rewards the generation of polymorphs in proportion to their appearance in the dataset. In this light, METRe can be thought of as a k -match rate where k is inferred from the number of polymorphs of each chemical composition in the test dataset. The efficiency gains come from the fact that none of the structures generated in the computation of METRe are discarded.

One potential downside of METRe with respect to k -match rate is the number of calls to PyMatGen’s `StructureMatcher` which are necessary. Since each reference structure and each generated structure must be compared, METRe has a worst-case time complexity of $\mathcal{O}(n^2)$. However, this is rarely the case as only materials with matching chemical stoichiometry can be matched. Structures with incongruent stoichiometry are automatically rejected making the algorithm computationally efficient in most practical settings.

B Data availability

The original *carbon-24* and *perov-5* datasets were released under the MIT license in the GitHub repository of CDVAE [15]: <https://github.com/txie-93>. We also release polymorph-split versions of *MP-20* [39] and *Alex-MP-20* [6, 49, 50] keeping polymorphs in the same split and ensuring that the distribution of *n*-arity—the number of unique elements *n* in each crystal structure—did not change between the combined dataset and each of the splits.

All datasets introduced in this work are released under the CC-BY 4.0 license on Huggingface under the following links:

- ***carbon-24-unique*** and ***carbon-24-unique-N-split*** — Dataset of unique carbon structures derived from the original *carbon-24* dataset treating enantiomorph pairs as duplicates: https://huggingface.co/datasets/colabfit/carbon-24_unique
- ***carbon-24-unique-with-enantiomorphs*** — Dataset of unique carbon structures derived from the original *carbon-24* dataset treating enantiomorph pairs as distinct: https://huggingface.co/datasets/colabfit/carbon-24_unique_with_enantiomorphs
- ***carbon-enantiomorphs*** — Only the 80 chiral pairs from *carbon-24-unique-with-enantiomorphs*, split into a train and validation set with opposite-handedness structures index-matched: <https://huggingface.co/datasets/colabfit/carbon-enantiomorphs>
- ***carbon-X*** — A dataset of one particular carbon crystal structure with fixed number of atoms *N* = 6 and lattice vectors *L* but under various translations of fractional coordinates *X*: https://huggingface.co/datasets/colabfit/carbon_X
- ***carbon-NXL*** — A dataset of one particular carbon crystal structure with different unit-cell representations that vary all *N*, *X*, and *L*: https://huggingface.co/datasets/colabfit/carbon_NXL
- ***perov-5-polymorph-split*** — New splits for the *perov-5* dataset which restrict polymorph pairs to be in the same part of each split: https://huggingface.co/datasets/colabfit/perov-5_polymorph_split
- ***MP-20-polymorph-split*** — New splits for the *MP-20* dataset which restrict polymorph pairs to be in the same part of each split: <https://huggingface.co/datasets/colabfit/MP-20-polymorph-split>
- ***Alex-MP-20-polymorph-split*** — New splits for the *Alex-MP-20* dataset which restrict polymorph pairs to be in the same part of each split: https://huggingface.co/datasets/colabfit/Alex-MP-20_Polymorph_Split

C Code availability

Pymatgen and its StructureMatcher are released under the MIT license: <https://github.com/materialsproject/pymatgen>

We additionally list links and licenses to the different open-source generative models that we evaluated in this work:

- DiffCSP [14] is released under the MIT license: <https://github.com/jiaor17/DiffCSP>
- FlowMM [12] is released under the CC-BY-NC license: <https://github.com/facebookresearch/flowmm>
- OMatG [5] is released under the MIT license: <https://github.com/FERMat-ML/OMatG>

D Hyperparameter choices

Hyperparameter selection is crucial to the performance of the three generative models that we investigated in this work. For FlowMM and DiffCSP, we chose the hyperparameters from these works which yielded the best performance for both the *carbon-24* and *perov-5* datasets [12, 14]. For OMatG, we performed hyperparameter optimization to minimize the CRMSE metric using the Ray

Tune package [51] along with the HyperOpt Bayesian optimization library [52]. For more details on the hyperparameter search spaces, see Höllmer et al. [5].

OMatG models discussed throughout this work are labeled by the interpolating function used to learn the fractional coordinates X . For more details on the functional forms of these interpolants, we refer to Albergo et al. [45] and Höllmer et al. [5].

Model checkpoints and accompanying hyperparameters for the OMatG models trained in this study will be accessible at: <https://huggingface.co/OMatG>

E Cost of training and optimization

Here we report the cost of model training for DiffCSP, FlowMM, and OMatG as well as hyperparameter optimization for OMatG [5, 12, 14]. For training on both *carbon*-24-unique- N -split datasets, we trained DiffCSP, FlowMM, and two versions of OMatG (standard and augmented) for 8000 epochs on either NVIDIA RTX8000, V100 or A100 GPUs. For training OMatG on *carbon-X* and *carbon-NXL* we trained one version with a standard CSPNet encoder and one with an augmented CSPNet encoder which breaks invariance to unit cell choice for 8000 epochs for each dataset on either NVIDIA RTX8000 or V100 GPUs.

For hyperparameter optimization of each different OMatG version on the *carbon*-24-unique, *perov-5*, and *perov-5*-polymorph-split datasets we trained on 2 NVIDIA A100 GPUs for 5 days for each model. For training DiffCSP and FlowMM on these three datasets we used NVIDIA A100 GPUs each for 8000, 6000, and 6000 epochs respectively.

F Crystallography primer

Crystallography deals with the study and classification of crystal structures. Idealized crystal structures are infinite point patterns which contain long-range translational periodic order.⁴

Lattices The translational symmetry of crystals is captured by their crystal *lattices* (also called Bravais lattices). There are five in two dimensions and fourteen in three dimensions.

A lattice can be described by the discrete set of points generated by integer linear combinations of a set of linearly independent basis vectors:

$$\Lambda = \{\mathbf{R} = n_1 \mathbf{a}_1 + n_2 \mathbf{a}_2 + n_3 \mathbf{a}_3 \mid n_i \in \mathbb{Z}\}.$$

The vectors $\mathbf{a}_1, \mathbf{a}_2, \mathbf{a}_3$ span the repeating unit of the lattice, called the *unit cell*, whose volume is given by

$$V_{\text{cell}} = |\mathbf{a}_1 \cdot (\mathbf{a}_2 \times \mathbf{a}_3)|.$$

Lattices should not be conflated with structures: for example, the commonly-referred to *fcc* (face-centered-cubic) is a lattice, and not a crystal structure; the crystal structure is termed monatomic *fcc* (sometimes termed cubic-close-packed, or *ccp*), where a particle sits directly on each lattice point. More generally, a crystal structure can be viewed as the combination of a Bravais lattice and a *basis* of particles attached to each lattice point:

$$\Lambda + \{\mathbf{r}_\alpha\}_{\alpha=1}^{N_{\text{basis}}},$$

where each \mathbf{r}_α specifies the position of an atom within the unit cell.

Space group symmetry In three dimensions, *space groups* combine translations with rotations, inversions/reflections, screw axes, and glide planes. The crystal space-group symmetry partitions space into sets of symmetry-equivalent points called Wyckoff positions. Each Wyckoff position is characterized by a site-symmetry group—the subgroup of the space group that leaves a representative point of that position fixed—and particles occupy one or more of these positions. Wyckoff positions can either be general (for arbitrary coordinates (x, y, z)) or special (possessing higher site-symmetry and reduced free parameters compared to the general position). For each space group, there are an infinite number of possible crystal structures. Crystals are classified by the full (maximal)symmetry space group of the structure, but they may also be represented by subgroups of their space group). For example, space group *P1* has one Wyckoff position with free parameters (x, y, z) —any crystal structure can be classified as space group *P1*, though this classification is not useful if the structure possesses higher symmetry.

Space group tables are available through the International Union of Crystallography (IUCr) [53]. Standard notations include Hermann–Mauguin (international), Schoenflies, and Hall symbols.

Unit cells Crystal structures can be defined by their *unit cell*, composed of the lattice vectors, the particle coordinates, and the chemical identities of the particles. A fully specified unit cell generates a unique periodic crystal structure, though a structure has many equivalent unit-cell representations. Degenerate representations can be related by unimodular transformations of the lattice vectors:

$$\mathbf{a}'_i = \sum_j M_{ij} \mathbf{a}_j, \quad M \in GL(3, \mathbb{Z}), \quad \det M = \pm 1.$$

These equations can be summarized as requiring volume preservation (through the allowed values of the determinant) and redefining the basis vectors by integer combinations of one another. These $GL(3, \mathbb{Z})$ changes are coordinate changes on the lattice, therefore $\det M = -1$ reverses the cell orientation but does not invert the physical crystal. We assume the number of particles in the cell is constant, therefore excluding supercells—which are yet another way to generate unit cells with different lattice vectors. In summary, the same physical crystal can be represented by infinitely many equivalent unit cells.

There are two types of standardized unit cells: conventional and primitive. The primitive cell is the smallest volume that, when translated by all lattice vectors $\mathbf{R} \in \Lambda$, fills all of space without overlaps

⁴We forego discussion of quasiperiodic order for the purposes of this primer.

or gaps, and contains exactly one lattice point.⁵ Primitive cells are not uniquely defined; however, the Niggli-reduced cell can be computed algorithmically [54] and is a unique choice of the primitive cell. Although the primitive cell is the minimal repeating unit of a crystal, the conventional cell is often preferred in crystallography because it makes the underlying symmetry of the lattice and crystal more explicit. Conventional cells are defined differently for each crystal system (*e.g.*, cubic, tetragonal, orthorhombic) to highlight characteristic symmetry axes and planes. This process of symmetrizing a unit cell from its primitive to conventional cell can be performed using the *spglib* software [55]. Although not standardized, *supercells* can be generated by replicating unit cells along lattice vectors to create larger periodic volumes—for example, to model defects or finite-size effects.

We walk through these concepts in a crystallography primer notebook with the *carbon-NXL* dataset, which is accessible at <https://www.kaggle.com/code/mayamartirossyan/crystal-representations-primer>

⁵One lattice point corresponds to the number of particles that are in the basis.

G Tolerance sensitivity analysis of cRMSE and METRe

We include results in Fig. 4 for benchmarking the tolerance sensitivity of both the METRe and cRMSE metrics on the changing of l_{tol} , $stol$, and $angle_tol$. Our results suggest a sensitivity to tolerance based on the match-quality of the generated structures, which is inferred from their performance metrics (METRe and cRMSE). Generated datasets with higher-quality matches are less sensitive to the `StructureMatcher` tolerance parameters. Moreover, across the board it is clear that $stol$ has the most impact in determining both METRe rate and cRMSE.

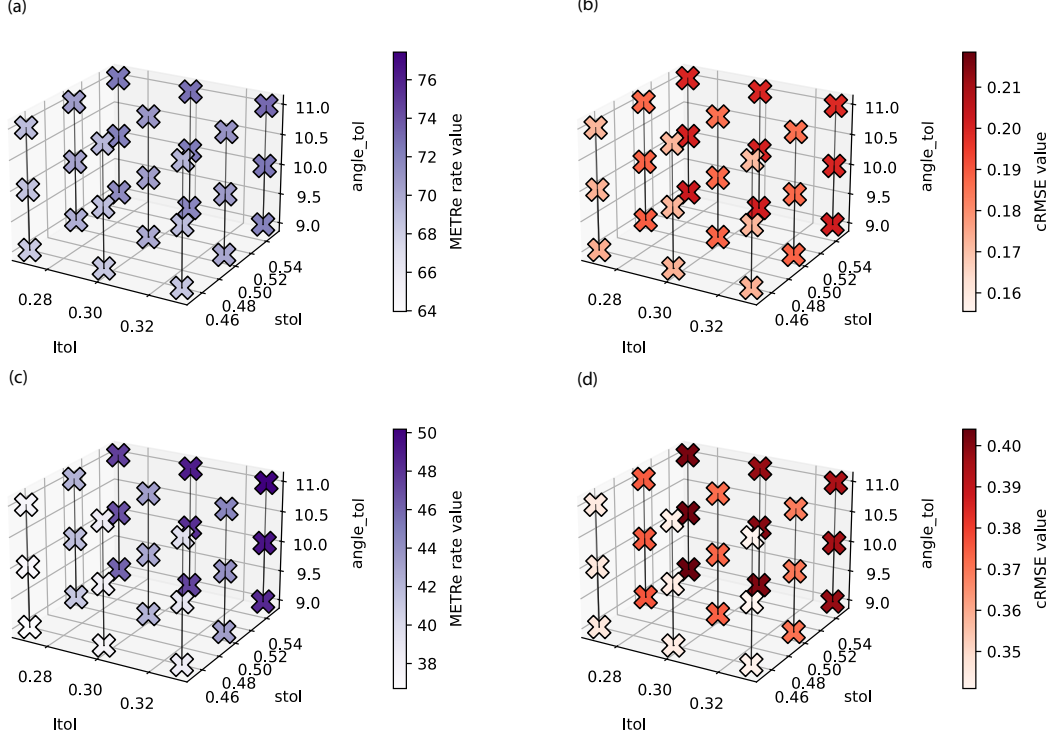


Figure 4: Tolerance sensitivity plots for OMatG models trained on the polymorph-split *MP-20* dataset. **(a–b)** Best-performing model with linear positional interpolant and ODE sampling and **(c–d)** worst-performing model with trigonometric interpolant with the latent variable γ and ODE sampling. METRe rates are shown for (a) and (c) and cRMSE values are shown for (b) and (d); color bars have equivalently-sized ranges across subfigures. Vertical lines are drawn for clarity.

H Additional discussion and evaluations on *carbon-24*-derived datasets

H.1 Evaluations on *carbon-X* and *carbon-24-unique-N-split*

We include below benchmarking results for *carbon-X* (Tab. 4) and the two *carbon-24-unique-N-split* dataset splits (Tab. 5).

The *carbon-X* match rate is 100% (Table 4), which is unsurprising given that both CSPNet and the OMatG model—which explicitly corrects for the system’s center-of-mass to make flows—are translation invariant. For *carbon-24-unique-N-split*, the split with low- N structures in the training set, combined with high- N structures in the test set, results in poor performance compared to both the high-to-low split as well as the *carbon-24-unique* dataset.

Table 4: Benchmarking *carbon-X* with mean RMSE, corrected mean cRMSE, and standard match rate because the dataset contains one unique crystal. The OMatG-LinearODE framework is used with two choices of encoders.

Model	<i>carbon-X</i>		
	Std. Match (%) \uparrow	RMSE \downarrow	cRMSE \downarrow
CSPNet	100.0 %	0.001	0.001
aug-CSPNet	100.0 %	0.001	0.001

Table 5: Benchmarking performance of generative models DiffCSP, FlowMM, and OMatG-LinearODE on the *carbon-24-unique-N-split* datasets with both increasing (low-to-high) and decreasing (high-to-low) atoms per unit cell N . Match rate and RMSEs are computed with the METRe metric.

Model	<i>carbon-24-unique-N-split</i> (low \rightarrow high)			<i>carbon-24-unique-N-split</i> (high \rightarrow low)		
	METRe (%) \uparrow	RMSE \downarrow	cRMSE \downarrow	METRe (%) \uparrow	RMSE \downarrow	cRMSE \downarrow
DiffCSP	96.7 %	0.426	0.429	100.0 %	0.077	0.077
FlowMM	97.4 %	0.404	0.406	100.0 %	0.043	0.043
OMatG	96.3 %	0.398	0.402	100.0 %	0.045	0.045

H.2 Re-evaluating *carbon-24-unique*

We perform re-evaluation on the *carbon-24-unique* dataset both in the context of uniqueness (Fig. 5).

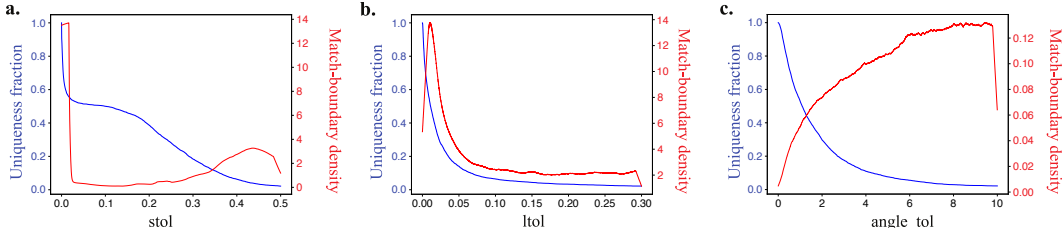


Figure 5: Tophat kernel density estimate of the distributions of match-boundary tolerance and uniqueness fraction for (a) $stol$, (b) $ltol$, and (c) $angle_tol$ performed on the *carbon-24-unique* dataset. These densities only count structure pairs which are considered matching at or below the maximum tolerances, and ignore structure pairs which are too structurally distinct to match.

In Fig. 5, we repeat the analysis of Section 3.1.1 on the *carbon-24-unique* dataset that was pruned of identified duplicates. As in Fig. 2 for the original *carbon-24* dataset, we show the distributions of the match-boundary tolerances for every tolerance parameter. In the deduplicated dataset, the large peak at low parameter values of $angle_tol$ is entirely gone. While there are still visible peaks for the other two parameters, these peaks are now shifted to higher tolerance values. Also, the increase of the estimated fraction of unique structure towards zero tolerances is less pronounced. The remaining presence of the peaks in the distributions for $stol$ and $ltol$ can be explained by our conservative

determination of duplicates, where two structures must be considered close with respect to all three tolerance parameters to be counted as a duplicate.

We do not directly compare generative models trained on datasets with duplicates and those trained on deduplicated datasets: Our reasoning for this is that both cases require a unified choice of a metric of sample quality and a shared test dataset. In our case, *carbon-24* and *carbon-24-unique* do not meet either criteria. For instance, consider benchmarking with METRe—which is the appropriate choice given the ‘polymorphism’ the carbon-only datasets exhibit, but is unsuitable to datasets with duplicate structures. Therefore, it would not provide a useful benchmark on the *carbon-24* dataset. Conversely, using the choice of standard match rate as a test metric is not informative because when polymorphs are present a one-to-one matching algorithm is not sensible.

While one could benchmark a model trained on a training set with duplicates on a deduplicated test dataset, care must be taken to ensure that there is no data leakage between the duplicated training set and the test dataset. In this work, we deduplicated the *carbon-24* dataset, and randomly split this into training, validation, and test datasets. Therefore, we did not ensure that the deduplicated test dataset and the original training set with duplicates do not have any crystal structures in common. Creating a shared test set is the clearest way to avoid data leakage, but is more straightforward to implement if one is augmenting a (deduplicated) dataset with duplicate structures; it is significantly more challenging to implement if de-duplication is required from a dataset containing duplicates, such as in our case.

We emphasize that datasets containing duplicates, including the original datasets, should be used where the prevalence of duplicate crystal structures is useful for the task at hand: for example, if one is attempting data augmentation for different unit cell representations. Therefore, training on duplicate structures is a completely reasonable objective as long as the presence of duplicate structures is documented and known.

H.3 Enantiomorphs

We benchmark the ability for our model to produce structures of different handedness by benchmarking model performance on the toy-dataset *carbon*-enantiomorphs, which is composed of only chiral carbon structures. The dataset is split into a training and validation set such that structures of opposite handedness are not in the same split. An OMatG model with linear positional interpolant was trained for 4000 epochs on the *carbon*-enantiomorphs training dataset, and the best validation loss checkpoint was used for generation. The model is then expected to generate either structures of the same or opposite handedness, and we investigate this by comparing METRe rate using two versions of `StructureMatcher`—one as-is and another which has improper rotations disabled. The latter is done by enabling the output of the rotation matrix found by the lattice mapping, and subsequently requiring that its determinant be positive.

Results are shown in Tab. 6. If the model memorized the training set structures, it would show poor performance with the inversion-disabled `StructureMatcher` and better performance with the standard `StructureMatcher` for comparisons between the generated structures and the validation set. In this case, the model was not especially successful at predicting even the correct structures, evident in poorer performance in comparison to the baseline set by the benchmarks comparing the training and validation structures with the inversion-disabled `StructureMatcher`. We note, however, that the similarity in the results between the generated structures *vs.* validation set and the generated structures *vs.* training set for both `StructureMatchers`. The results suggest a very modest preference for handedness learned and poor performance across the board.

Table 6: Six comparisons of structures measured with METRe, RMSE, and cRMSE. Both the standard implementation of `StructureMatcher` as well as an inversion-disabled version of it are utilized. The comparisons of the training and validation sets serve as a baseline for interpreting results.

	METRe (%) \uparrow	RMSE \downarrow	cRMSE \downarrow
Standard <code>StructureMatcher</code>			
Generated structures <i>vs.</i> validation set	90.0%	0.347	0.362
Generated structures <i>vs.</i> training set	90.0%	0.348	0.363
Training set <i>vs.</i> validation set	100.0%	0.003	0.003
Inversion-disabled <code>StructureMatcher</code>			
Generated structures <i>vs.</i> validation set	90.0%	0.358	0.372
Generated structures <i>vs.</i> training set	90.0%	0.356	0.371
Training set <i>vs.</i> validation set	100.0%	0.217	0.217

I Quantifying uncertainty for benchmarks

Below we provide standard error values from multiple generation runs with different seeds for *carbon-24-unique* (Table 7), *perov-5-polymorph-split* (Table 8), both *carbon-24-unique- N -split* low-to-high and high-to-low (Table 9), *carbon-NXL* (Table 10), and *carbon-X* (Table 11). We also include results for a modification of *carbon-X* in Table 12, in which six additional unit cells of the same crystal structure but with $N = 12$ carbon atoms are added during training to the existing 479 structures, but generation results are presented only for $N = 6$ atoms; we note the order of magnitude worse performance compared to Table 11. We use three generation runs as done *via* Miller et al. [12] for all tables excepting Table 10, 11, and 12.

Table 7: Standard errors for three generation runs from the same checkpoints reported for METRe, RMSE, and cRMSE values for the *carbon-24-unique* dataset.

Method	<i>carbon-24-unique</i>		
	METRe % (\uparrow)	RMSE (\downarrow)	cRMSE (\downarrow)
DiffCSP	98.0 \pm 0.2 %	0.229 \pm 0.001	0.234 \pm 0.001
FlowMM	98.1 \pm 0.1 %	0.1930 \pm 0.0003	0.199 \pm 0.001
OMatG-LinearODE	97.6 \pm 0.2 %	0.181 \pm 0.001	0.189 \pm 0.001
OMatG-LinearODE γ	97.7 \pm 0.3 %	0.212 \pm 0.001	0.219 \pm 0.001
OMatG-TrigODE	98.3 \pm 0.1 %	0.1825 \pm 0.0005	0.1880 \pm 0.0005
OMatG-TrigODE γ	98.1 \pm 0.1 %	0.180 \pm 0.001	0.187 \pm 0.002
OMatG-EncDecODE	98.5 \pm 0.1 %	0.200 \pm 0.003	0.205 \pm 0.002
OMatG-SBDODE	97.8 \pm 0.1 %	0.218 \pm 0.001	0.225 \pm 0.001

Table 8: Standard errors for three generation runs from the same checkpoints reported for METRe, RMSE, and cRMSE values for the *perov-5-polymorph-split* dataset.

Method	<i>perov-5-polymorph-split</i>		
	METRe % (\uparrow)	RMSE (\downarrow)	cRMSE (\downarrow)
DiffCSP	77.4 \pm 0.8 %	0.069 \pm 0.001	0.166 \pm 0.003
FlowMM	78.2 \pm 0.3 %	0.071 \pm 0.001	0.165 \pm 0.002
OMatG-LinearODE	76.8 \pm 0.1 %	0.0555 \pm 0.0003	0.1593 \pm 0.0005
OMatG-LinearODE γ	75.9 \pm 0.1 %	0.0670 \pm 0.0002	0.1713 \pm 0.0003
OMatG-TrigODE	76.7 \pm 0.3 %	0.0586 \pm 0.0003	0.161 \pm 0.001
OMatG-TrigODE γ	76.0 \pm 0.2 %	0.0529 \pm 0.0004	0.160 \pm 0.001
OMatG-EncDecODE	74.9 \pm 0.2 %	0.058 \pm 0.001	0.169 \pm 0.001
OMatG-SBDODE	76.7 \pm 0.5 %	0.061 \pm 0.001	0.163 \pm 0.001

Table 9: Standard errors for three generation runs from the same checkpoints reported for METRe, RMSE, and cRMSE values for the *carbon-24-unique- N -split* datasets.

Method	<i>carbon-24-unique-N-split</i> (low \rightarrow high)			<i>carbon-24-unique-N-split</i> (high \rightarrow low)		
	METRe (%) \uparrow	RMSE \downarrow	cRMSE \downarrow	METRe (%) \uparrow	RMSE \downarrow	cRMSE \downarrow
DiffCSP	96.7 \pm 0.1 %	0.4257 \pm 0.0005	0.428 \pm 0.001	100.0 \pm 0.0 %	0.083 \pm 0.005	0.083 \pm 0.005
FlowMM	97.8 \pm 0.2 %	0.4044 \pm 0.0004	0.4066 \pm 0.0003	100.0 \pm 0.0 %	0.0420 \pm 0.0004	0.0420 \pm 0.0004
OMatG-LinearODE	96.1 \pm 0.4 %	0.3974 \pm 0.0005	0.4014 \pm 0.0002	100.0 \pm 0.0 %	0.047 \pm 0.001	0.047 \pm 0.001

Table 10: Standard errors for 350 generation runs from the same checkpoints reported for METRe, RMSE, and cRMSE values for the *carbon-NXL* dataset. For breakdowns by number of atoms per unit cell N : there are 196 generation runs for $N = 6$, and 124 generation runs for $N = 8$.

Model	<i>carbon-NXL</i>						$N = 8$		
	All N			$N = 6$					
	Std. Match	RMSE \downarrow	cRMSE \downarrow	Std. Match	RMSE \downarrow	cRMSE \downarrow	Std. Match	RMSE \downarrow	cRMSE \downarrow
CSPNet	47.3 %	0.008 ± 0.001	0.266 ± 0.013	60.0 %	0.005 ± 0.001	0.203 ± 0.017	39.0 %	0.013 ± 0.003	0.310 ± 0.022
aug-CSPNet	47.7 %	0.006 ± 0.001	0.264 ± 0.013	69.2 %	0.005 ± 0.001	0.157 ± 0.016	26.0 %	0.010 ± 0.004	0.373 ± 0.019

Table 11: Standard errors for 479 generations from the same checkpoints reported for METRe, RMSE, and cRMSE values for the *carbon-X* dataset.

Model	Std. Match (%) \uparrow	<i>carbon-X</i>	
		RMSE \downarrow	cRMSE \downarrow
CSPNet	100.0 %	$0.0007 \pm 1 \times 10^{-5}$	$0.0007 \pm 1 \times 10^{-5}$
aug-CSPNet	100.0 %	$0.0007 \pm 1 \times 10^{-5}$	$0.0007 \pm 1 \times 10^{-5}$

Table 12: Standard errors for 479 generations with $N = 6$ from the same checkpoints reported for METRe, RMSE, and cRMSE values for a modified *carbon-X* dataset, in which six additional unit cells of the same crystal structure—but with $N = 12$ atoms—have been added during training. We note the surprising discrepancy added by the addition of these six structures during training and generation for only $N = 6$ atoms.

Model	Std. Match (%) \uparrow	<i>carbon-X-mod</i>	
		RMSE \downarrow	cRMSE \downarrow
CSPNet	100.0 %	0.060 ± 0.005	0.060 ± 0.006
aug-CSPNet	100.0 %	0.084 ± 0.005	0.084 ± 0.006

J Binary search algorithm for determining match-boundary

We address the question of distinctness using the following method: within the *carbon-24* dataset, all structures are compared to one another using the `StructureMatcher` with variable tolerance. For the upper triangular of the $10\ 153 \times 10\ 153$ matrix of structure comparisons, we calculate the tolerance at which the structure pairs from each row and column transition from matching to non-matching (the match-boundary) for each of `stol`, `ltol`, and `angle_tol`. Matches can be rejected for one of two reasons: if the choice of `stol` is lower than the RMSE of the match, or if there is significant structural dissimilarity such that no tolerance is sufficiently large in order to be considered matching. We find the tolerance at the match-boundary using a binary search method, except in the case of `stol`, where the binary search method is not necessary since the output RMSE from `StructureMatcher` is itself the `stol` at the match-boundary (we validated this by computing the matrix with using `stol` binary search). For each varied tolerance, the other two are held constant at the standard settings used in benchmarking generative models.

Below we provide the binary search algorithm utilized to find the tolerance at the match-boundary for a given pair of structures. We utilized 16 CPUs over approximately 3 days in order to compute the match-boundary tolerance for `ltol` and `angle_tol` (for a total of ≈ 1150 CPU hours per tolerance) and approximately 2 days for `stol` (for a total of ≈ 770 CPU hours).

```
import numpy as np
from pymatgen.analysis.structure_matcher import StructureMatcher

def binary_search(s1, s2, tol_to_test, thresh=1e-4):
    """ Returns value of tol_to_test at match boundary for PyMatGen
    Structure types s1 and s2"""
    # Set L (left boundary) to 0 for all three tolerances
    L = 0

    # Ensure tol_to_test is a string and assert that it be an allowed
    # option
    tol_to_test = str(tol_to_test)
    assert tol_to_test in ["ltol", "stol", "atol"]

    # For stol, the output RMSE is the value at the match-boundary
    if tol_to_test == "stol":
        # set other two tolerances loosely
        ltol = 0.3
        angle_tol = 10.
        # set R to be loosest tolerance for stol
        R = 0.5

        sm = StructureMatcher(ltol=ltol, stol=R, angle_tol=angle_tol)
        res = sm.get_rms_dist(s1, s2)
        if res is None:
            # return R=0.5 if there is no match
            return R
        else:
            # return the RMSE if there is a match
            return res[0]

    # binary-search for ltol or atol
    if tol_to_test == "ltol":
        # set other two tolerances loosely
        stol = 0.5
        angle_tol = 10.
        # set R to be loosest tolerance for ltol
        R = 0.3

        sm = StructureMatcher(ltol=R, stol=stol, angle_tol=angle_tol)
        res = sm.get_rms_dist(s1, s2)
        if res is None:
            # return R=0.3 if no match on first try
            return R
```

```

# enter while loop if matched on first try
while L < R:
    mid = (L + R) / 2
    # use new value of ltol at midpoint between L and R
    sm = StructureMatcher(ltol=mid, stol=stol, angle_tol=
        angle_tol)
    res = sm.get_rms_dist(s1, s2)
    # if R and L are close enough return R
    if np.abs(R-L) <= thresh:
        return R
    # if match, move R to be at midpoint
    elif res is not None:
        R = mid
    # if not matching, move L to be at midpoint
    elif res is None:
        L = mid

# binary-search for atol
if tol_to_test == "atol":
    # set other two tolerances loosely
    ltol = 0.3
    stol = 0.5
    # set R to be loosest tolerance for atol
R = 10.

sm = StructureMatcher(ltol=ltol, stol=stol, angle_tol=R)
res = sm.get_rms_dist(s1, s2)
if res is None:
    # return R=10. if no match on first try
    return R
# enter while loop if matched on first try
while L < R:
    mid = (L + R) / 2
    sm = StructureMatcher(ltol=ltol, stol=stol, angle_tol=mid)
    res = sm.get_rms_dist(s1, s2)
    # if R and L are close enough return R
    if np.abs(R-L) <= thresh:
        return R
    # if match, move R to be at midpoint
    elif res is not None:
        R = mid
    # if not matching, move L to be at midpoint
    elif res is None:
        L = mid

```